Unpaired Image Deraining Using Reward-Guided Self-Reinforcement Strategy

Supplementary Material

In this paper, we propose a novel **R**eward-**G**uided **S**elf-reinforcement **U**nsupervised Image **D**eraining framework, **RGSUD**, to address the lack of paired data by exploiting internal implicit deraining supervision and external VLM knowledge. Extensive experiments on multiple synthetic and real-world datasets verify that our method achieves excellent deraining performance. What's more, as shown in Figure 1 our RGSUD achieves the most promising performance on the real-world captured images compared to both supervised and unsupervised deraining methods, which demonstrates strong generalization capability of our RGSUD. This supplementary material mainly includes the following contents:

- Detailed Network Structures.;
- More Explanation of Ablation Setting;
- More Explanation of Self-Reinforcement Strategy;
- Dataset Description;
- Implementation Details;
- More Experiment Results;
- Discussion and limitations of our method.

1. Detailed Network Structures

As described in the main document, the proposed RGSUD mainly consists of a derainer, a generator, and a discriminator. To balance the performance and computational complexity, we adopt the simple CNN-based image restoration baseline NAFNet [1] (the version of width32) as the default derainer.

1.1. Architecture of the Generator

The purpose of the generator is to synthesize a rainy image that matches the real rain distribution from a clean image. The generative network architecture is shown in Figure 2. Specifically, three convolutional layers followed by LeakyReLU are contained at both the beginnings and end of the network. In addition, six convolutional residual blocks are included in the middle part of the generator

1.2. Architecture of the Discriminator

In our network, we use a Patch-GAN [26] discriminator, as shown in Fig. 6. The discriminator is starting with a 4×4 convolution layer with ReLU activation function, followed by three intermediate layers, each of which consists of instance normalization between the convolution layer and the activation function, and ending with a 4×4 convolution layer with a stride of 1.

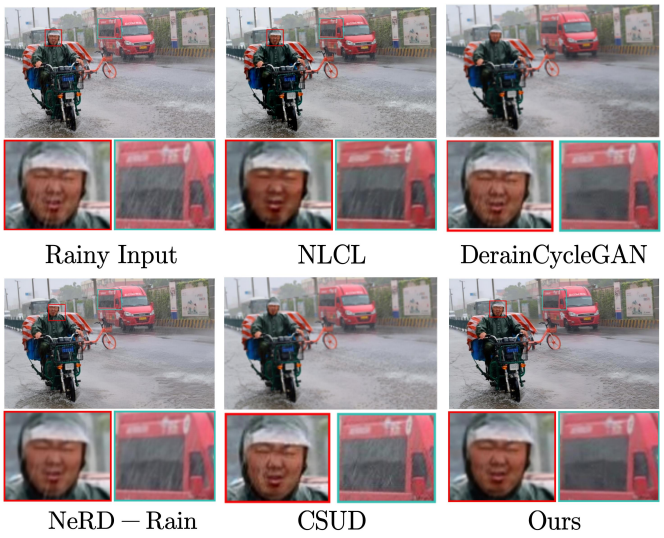

Figure 1. Deraining results on the real rainy images captured by ourselves in real-world scenarios. Compared with the supervised method NeRD-Rain [4] and the unsupervised method DerainCycleGAN [18], our RGSUD exhibits extremely strong generalization capability and achieves the best visual results.

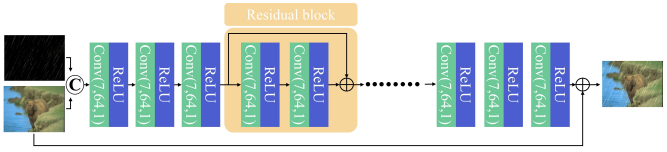

Figure 2. Detailed network structures of the generator.

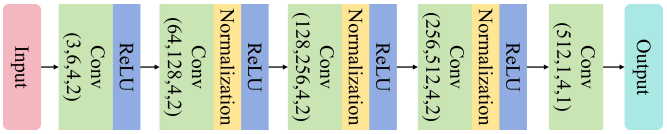

Figure 3. Detailed network structures of the discriminator.

2. More Explanation of Ablation Setting

As described in the main document, we separately validated the transferability of the network architecture and the proposed self-reinforcement (SR) training strategy. For the former, we separately replaced the original NAFNet derainer with Restormer [23], DRSformer [3], and NeRD-Rain [4], and then retrained them using the same training process on the Rain200L, SPA-Data, and RealRain1K-L datasets. The experimental results indicate that the original NAFNet network is the most effective derainer. Furthermore, our self-reinforcement training is effective on the three different de-

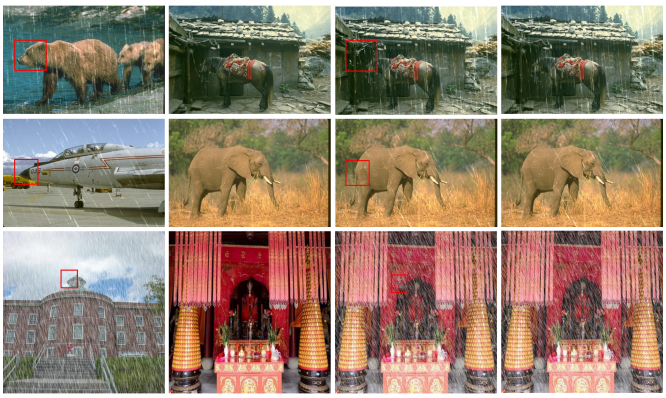

Figure 4. The effects of SR strategy on the performance of generator. The first and second columns present the input rainy and clean images of the generator, respectively; the third column presents pseudo rainy images generated by the generator without SR strategy; the fourth column presents pseudo rainy images generated by the generator with SR strategy.

rainer network structures mentioned. For the latter, to validate the applicability of the proposed training strategy, we conducted experimental verification on classical unpaired unsupervised deraining methods, including: DCDGAN [2], DerainCycleGAN [18], NLCL [21] and CSUD [6]. Specifically, we continue to follow a two-stage training approach, which consists of rewards recycling and self-reinforcement (SR) strategy training. Because our reward recycling mechanism is plug-and-play, it is independent of the specific network architecture. In the self-reinforcement training, we only consider using the self-reinforcement loss to constrain the network's optimization space, and do not consider the improvement of pseudo-paired data synthesis by the rewards. Because not every unpaired deraining method involves pseudo-paired data synthesis. Some methods, like NLCL [21], strive to constrain the optimization space from a feature space perspective by leveraging the contrastive learning paradigm.

3. More Explanation of Self-Reinforcement Strategy

As described in main document, in the self-reinforcement training stage, we utilize the derainer's outputs (rewards) to compute more accurate degradation information and synthesize higher-quality pseudo-paired data. Additionally, as shown in Figure 4, we present more visualizations of the effects of SR strategy on the performance of generator G. With SR strategy, the generator effectively alleviates the redundant information transfer problem, ensuring that higher-quality pseudo rainy images are generated.

4. Dataset Description

To fully evaluate the effectiveness of our method in complex rain scenes, we adopt six benchmark datasets. Rain100L datasets contain 200 training frames and 100 testing frames. Rain200L [20] datasets contain 1,800 synthetic rainy images for training and 200 ones for testing. DID-Data [25] and DDN-Data [7] consist of 12,000 and 12,600 synthetic images with different rain directions and density levels. There are 1,200 and 1,400 rainy images for testing. SPA-Data [16] is the paired real-world dataset which utilizes the human-supervised percentile video filtering to obtain the ground turths. It contains 638,492 rainy/clear image patches for training and 1,000 testing ones. RealRain1K-L [10] contains 1120 rainy and clear frame pairings, which are divided into 784 training frames, 224 test frames and 112 validation frames. SIRR [17] contains 147 outdoor rainy images and Rain3000 [12] has 300 really rainy images. The detailed descriptions of the used training and testing datasets are tabulated in Table 1.

Table 1. Detailed description of the datasets utilized.

Datasets	Rain100L [20]	Rain200L [20]	DID-Data [25]	DDN-Data [7]	RealRain1K-L [10]
Train	200	1800	12000	12600	784
Test	100	200	1200	1400	224
Rain Type	Synthetic	Synthetic	Synthetic	Synthetic	Real-world

Datasets	SPA-data [16]	Rain3000 [12]	SIRR [17]	Night-Rain [24]
Train	638,492	2700	0	5000
Test	1000	300	147	500
Rain Type	Real-world	Real-world	Real-world	Night-Time

5. Implementation Details

Our methodology is executed using the PyTorch [14] platform, conducted on a system powered by four NVIDIA Tesla V100 GPUs. For the training phase, we adopt the Adam [5] optimizer algorithm with $\beta_1 = 0.9$, $\beta_2 = 0.999$, and the initial learning rate is set to 2×10^{-4}. All training images undergo random cropping into 256 × 256 patches in an unpaired manner. The hyperparameters λ_1, λ_2 are set to 1.0 and 0.8, respectively. For fair comparison, all PSNR and SSIM scores reported in the main document are calculated on the RGB channels. The results of other methods are directly cited from the original papers or generated using the official models. For the results on datasets that the authors did not report or test, we retrain their models using the official code provided by the authors.

6. More Experiment Results

We present more experiment results on unsupervised deraining performance and generalization performance to further elucidate the effectiveness of the proposed RGSUD.

6.1. Unsupervised Deraining Results

We provide additional visual comparisons on benchmark datasets in Figure 5. We compare our RGSUD with several recent state-of-the-art unsupervised and supervised im-

Table 2. Downstream tasks evaluation.

	Semantic Segmentation				Object Detection			
	RainCityscape [8]		Rain100L [20]		Rain100L [20]		DID-Data [25]	
Methods	mAcc↑	mIou↑	mAcc↑	mIou↑	mAP50↑	mAP75↑	mAP50↑	mAP75↑
DerainCycleGAN [18]	61.09	54.81	74.12	63.50	94.24	68.04	82.21	54.82
DCD-GAN [2]	61.93	55.71	73.76	62.69	93.03	67.21	80.58	54.22
CSUD [6]	65.97	58.41	74.76	63.13	95.00	69.18	83.71	56.91
Ours	67.17	60.50	79.04	68.03	96.03	72.07	86.27	59.71

Table 3. Potential Biases.

Dataset	Dog-IQA [11]	DeQA-Score [22]	Q-Align [19]	DACLIP-IQA [13]
Rain100L [20]	82.9%	83.6%	85.4%	92.7%
Night-Rain [24]	72.1%	74.2%	75.6%	87.3%
RealRain1K-L [10]	75.7%	81.2%	79.8%	88.6%

age deraining methods. As shown in the figures, it can be seen that our RGSUD achieves better results in removing rain streaks compared to other unsupervised methods and our RGSUD preserves more texture details of image background.

6.2. Generalization Deraining Results

To validate the generalization capability of RGSUD, we provide more additional visual comparisons with other unsupervised and supervised deraining methods, in Figure 6 and Figure 7. All methods are trained on synthetic datasets and tested on the unseen real-world datasets. Compared to other methods, our RGSUD achieves better visual results in real-world scenarios, which demonstrates the excellent generalization capability of RGSUD.

6.3. Evaluation on Downstream Tasks

As shown in Table 2, we report quantitative downstream results for semantic segmentation (RainCityscape, Rain100L with SAM [9]) and object detection (Rain100L, DID-Data with DINO-X [15]). Since the Rain100L dataset does not provide ground truth segmentation masks, we employed the SAM (Segment Anything Model) to extract precise masks from the rain-free images. These were then utilized as ground truth labels for quantitative evaluation. Given the current lack of publicly available datasets specifically designed for object detection in rainy conditions, we utilized DINO-X, a large-scale object detection model, to generate detection results. These results were subsequently formatted into documents compatible with YOLO to serve as ground truth labels.

6.4. Potential Biases and VLM-based IQA

In Table 3, we evaluate bias and rain sensitivity of VLM-based IQA using quality-controlled samples $\alpha_i x^l + (1-\alpha_i) \times y^l{}_{i=1}^{10}$ ($\alpha_i = 0.1 \times i$), whose quality degrades monotonically. This tests how well VLM-IQA preserves monotonicity. As shown in Table 4, DACLIP-IQA offers more stable guidance than Q-align and DeQA-Score under low-light and heavy-rain conditions. (x^l and y^l: paired rainy and clean image)

Table 4. Result of VLM-based IQA.

VLM based IQA	Dog-IQA [11]		DeQA-Score [22]		Q-align [19]		DACLIP-IQA [13]	
	PSNR↑	SSIM↑	PSNR↑	SSIM↑	PSNR↑	SSIM↑	PSNR↑	SSIM↑
Rain100L [20]	33.73	0.957	33.83	0.964	33.87	0.962	34.41	0.967
Night-Rain [24]	29.03	0.865	29.12	0.871	29.14	0.873	30.54	0.897
RealRain1K-L [10]	31.96	0.951	32.04	0.953	31.88	0.946	32.88	0.955

Table 5. Initialization.

Train Epoch (Rain100L [20])	Stage I			Stage II			Improvement	
	PSNR↑	SSIM↑	Times	PSNR↑	SSIM↑	Times	PSNR↑	SSIM↑
100	29.89	0.865	7.3h	32.85	0.941	2h	2.96	0.076
150	31.51	0.932	10.9h	34.15	0.959	2h	2.64	0.027
250	32.52	0.943	18.1h	34.22	0.958	2h	1.7	0.015
350	33.04	0.949	24.8	34.41	0.967	2h	1.37	0.018

6.5. Impact of Initial Rain Removal Results

As shown in Table 5, we start Stage II from different Stage I checkpoints on Rain100L (100–350 epochs). In all cases, Stage II brings clear PSNR/SSIM gains (*e.g.,* 29.89/0.865→32.85/0.941 and up to 33.04/0.949→34.41/0.967) with the same two-hour cost. Thus, our self-reinforcement strategy is robust even to weak initial deraining, while stronger initialization naturally yields slightly better final performance.

7. Discussion and limitations of our method.

Our approach is currently limited to the image deraining task. Other restoration tasks, such as low-light enhancement and deblurring, often do not adhere to additive degradation modeling; consequently, the synthesis of pseudo-paired data requires additional consideration of the complex interactions between features. In addition, robust and sensitive image quality assessment (IQA) metrics are crucial. Consequently, large vision-language models (LVLMs) fine-tuned on specific tasks or scenarios can further enhance the image reconstruction performance of the algorithm. Finally, the coexistence of multiple degradations is a common occurrence in real-world scenarios. Exploring more diverse perception of these degradations and integrating such mechanisms with our proposed method remains a key direction for future research.

References

[1] Liangyu Chen, Xiaojie Chu, Xiangyu Zhang, and Jian Sun. Simple baselines for image restoration. In *European conference on computer vision*, pages 17–33. Springer, 2022. 1

[2] Xiang Chen, Jinshan Pan, Kui Jiang, Yufeng Li, Yufeng Huang, Caihua Kong, Longgang Dai, and Zhentao Fan. Unpaired deep image deraining using dual contrastive learning. In *Proceedings of the IEEE/CVF conference on computer vision and pattern recognition*, pages 2017–2026, 2022. 2, 3

[3] Xiang Chen, Hao Li, Mingqiang Li, and Jinshan Pan. Learning a sparse transformer network for effective image deraining. In *Proceedings of the IEEE/CVF conference on computer vision and pattern recognition*, pages 5896–5905, 2023. 1

[4] Xiang Chen, Jinshan Pan, and Jiangxin Dong. Bidirectional multi-scale implicit neural representations for image deraining. In *Proceedings of the IEEE/CVF conference on com-*

Figure 5. Qualitative generalization results on Rain200L [20] dataset.

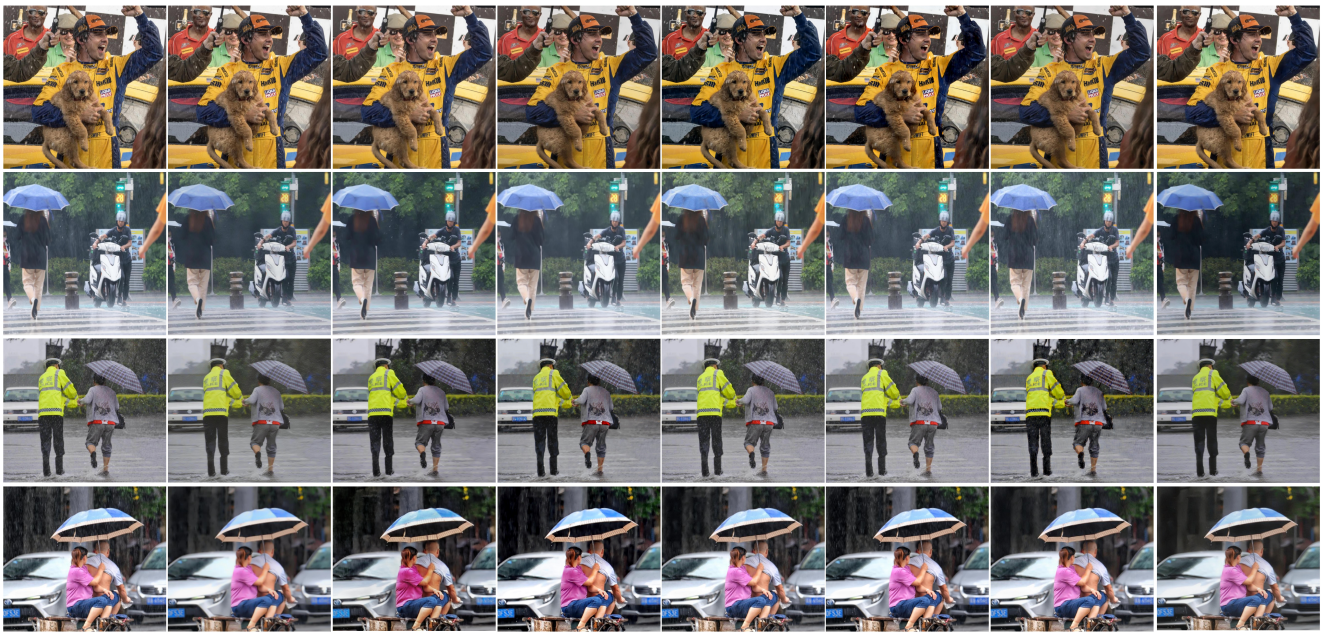

Figure 6. Qualitative generalization results on Rain3000 [12] dataset.

puter vision and pattern recognition, pages 25627–25636, 2024. 1

[5] P Kingma Diederik. Adam: A method for stochastic optimization. *(No Title)*, 2014. 2

[6] Guanglu Dong, Tianheng Zheng, Yuanzhouhan Cao, Linbo Qing, and Chao Ren. Channel consistency prior and self-reconstruction strategy based unsupervised image deraining. In *Proceedings of the Computer Vision and Pattern Recognition Conference*, pages 7469–7479, 2025. 2, 3

[7] Xueyang Fu, Jiabin Huang, Delu Zeng, Yue Huang, Xinghao Ding, and John Paisley. Removing rain from single images via a deep detail network. In *Proceedings of the IEEE conference on computer vision and pattern recognition*, pages 3855–3863, 2017. 2

[8] Xiaowei Hu, Chi-Wing Fu, Lei Zhu, and Pheng-Ann Heng. Depth-attentional features for single-image rain removal. In *Proceedings of the IEEE/CVF Conference on Computer Vision and Pattern Recognition (CVPR)*, 2019. 3

[9] Alexander Kirillov, Eric Mintun, Nikhila Ravi, Hanzi Mao, Chloe Rolland, Laura Gustafson, Tete Xiao, Spencer Whitehead, Alexander C Berg, Wan-Yen Lo, et al. Segment anything. In *Proceedings of the IEEE/CVF international conference on computer vision*, pages 4015–4026, 2023. 3

[10] Wei Li, Qiming Zhang, Jing Zhang, Zhen Huang, Xinmei

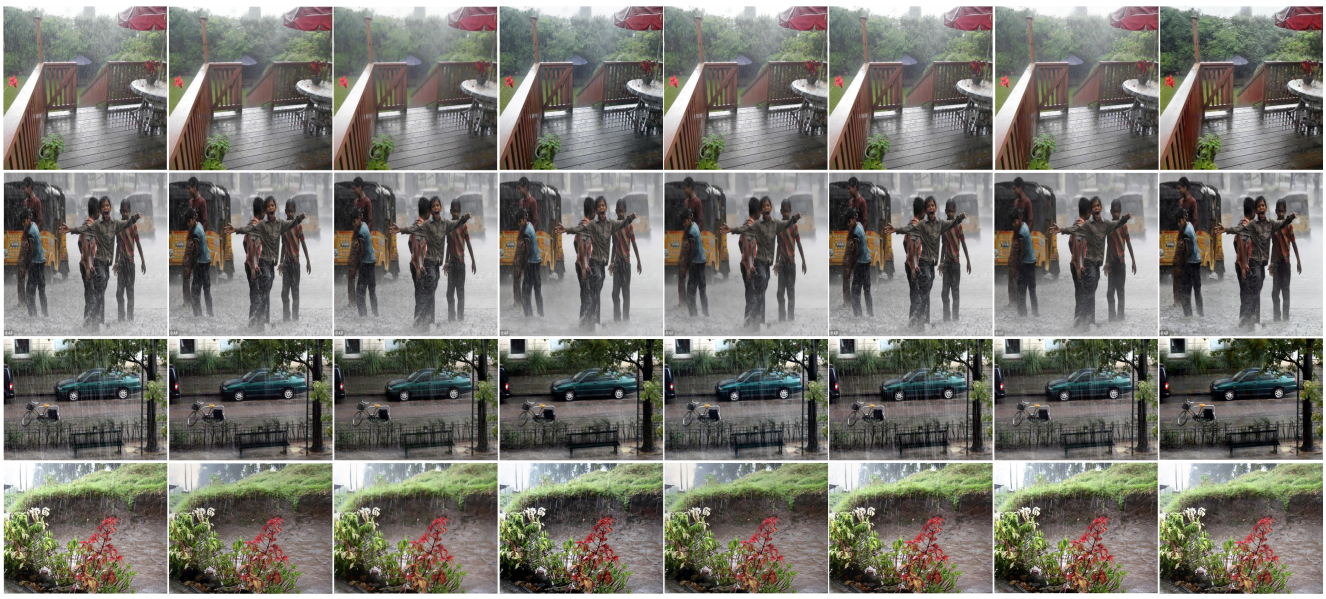

(a) Input (b) DerainCycleGAN (c) DCD-GAN (d) NLCL (e) DRSformer (f) NeRD-Rain (g) CSUD (h) Ours

Figure 7. Qualitative generalization results on SIRR [17] dataset.

Tian, and Dacheng Tao. Toward real-world single image deraining: A new benchmark and beyond. *arXiv preprint arXiv:2206.05514*, 2022. 2, 3

[11] Kai Liu, Ziqing Zhang, Wenbo Li, Renjing Pei, Fenglong Song, Xiaohong Liu, Linghe Kong, and Yulun Zhang. Dog-iqa: Standard-guided zero-shot mllm for mix-grained image quality assessment, 2024. 3

[12] Yang Liu, Ziyu Yue, Jinshan Pan, and Zhixun Su. Unpaired learning for deep image deraining with rain direction regularizer. In *Proceedings of the IEEE/CVF international conference on computer vision*, pages 4753–4761, 2021. 2, 4

[13] Ziwei Luo, Fredrik K Gustafsson, Zheng Zhao, Jens Sjölund, and Thomas B Schön. Controlling vision-language models for multi-task image restoration. In *International Conference on Learning Representations*, 2024. 3

[14] Adam Paszke, Sam Gross, Francisco Massa, Adam Lerer, James Bradbury, Gregory Chanan, Trevor Killeen, Zeming Lin, Natalia Gimelshein, Luca Antiga, et al. Pytorch: An imperative style, high-performance deep learning library. *Advances in neural information processing systems*, 32, 2019. 2

[15] Tianhe Ren, Yihao Chen, Qing Jiang, Zhaoyang Zeng, Yuda Xiong, Wenlong Liu, Zhengyu Ma, Junyi Shen, Yuan Gao, Xiaoke Jiang, Xingyu Chen, Zhuheng Song, Yuhong Zhang, Hongjie Huang, Han Gao, Shilong Liu, Hao Zhang, Feng Li, Kent Yu, and Lei Zhang. Dino-x: A unified vision model for open-world object detection and understanding, 2025. 3

[16] Tianyu Wang, Xin Yang, Ke Xu, Shaozhe Chen, Qiang Zhang, and Rynson WH Lau. Spatial attentive single-image deraining with a high quality real rain dataset. In *Proceedings of the IEEE/CVF conference on computer vision and pattern recognition*, pages 12270–12279, 2019. 2

[17] Wei Wei, Deyu Meng, Qian Zhao, Zongben Xu, and Ying Wu. Semi-supervised transfer learning for image rain removal. In *Proceedings of the IEEE/CVF conference on computer vision and pattern recognition*, pages 3877–3886, 2019. 2, 5

[18] Yanyan Wei, Zhao Zhang, Yang Wang, Mingliang Xu, Yi Yang, Shuicheng Yan, and Meng Wang. Deraincyclegan: Rain attentive cyclegan for single image deraining and rainmaking. *IEEE Transactions on Image Processing*, 30:4788–4801, 2021. 1, 2, 3

[19] Haoning Wu, Zicheng Zhang, Weixia Zhang, Chaofeng Chen, Liang Liao, Chunyi Li, Yixuan Gao, Annan Wang, Erli Zhang, Wenxiu Sun, et al. Q-align: Teaching lmms for visual scoring via discrete text-defined levels. *arXiv preprint arXiv:2312.17090*, 2023. 3

[20] Wenhan Yang, Robby T Tan, Jiashi Feng, Jiaying Liu, Zongming Guo, and Shuicheng Yan. Deep joint rain detection and removal from a single image. In *Proceedings of the IEEE conference on computer vision and pattern recognition*, pages 1357–1366, 2017. 2, 3, 4

[21] Yuntong Ye, Changfeng Yu, Yi Chang, Lin Zhu, Xi-Le Zhao, Luxin Yan, and Yonghong Tian. Unsupervised deraining: Where contrastive learning meets self-similarity. In *Proceedings of the IEEE/CVF conference on computer vision and pattern recognition*, pages 5821–5830, 2022. 2

[22] Zhiyuan You, Xin Cai, Jinjin Gu, Tianfan Xue, and Chao Dong. Teaching large language models to regress accurate image quality scores using score distribution. In *Proceedings of the Computer Vision and Pattern Recognition Conference*, pages 14483–14494, 2025. 3

[23] Syed Waqas Zamir, Aditya Arora, Salman Khan, Munawar Hayat, Fahad Shahbaz Khan, and Ming-Hsuan Yang. Restormer: Efficient transformer for high-resolution image restoration. In *Proceedings of the IEEE/CVF conference on*

computer vision and pattern recognition, pages 5728–5739, 2022. 1

[24] Fan Zhang, Shaodi You, Yu Li, and Ying Fu. Learning rain location prior for nighttime deraining and beyond. *IEEE Transactions on Pattern Analysis and Machine Intelligence*, 47(10):9169–9186, 2025. 2, 3

[25] He Zhang and Vishal M Patel. Density-aware single image de-raining using a multi-stream dense network. In *Proceedings of the IEEE conference on computer vision and pattern recognition*, pages 695–704, 2018. 2, 3

[26] Jun-Yan Zhu, Taesung Park, Phillip Isola, and Alexei A Efros. Unpaired image-to-image translation using cycle-consistent adversarial networks. In *Proceedings of the IEEE international conference on computer vision*, pages 2223–2232, 2017. 1